Air lasing from singly ionized N_2 driven by bicircular two-color fields

Hanxiao Li,[1] Qiying Song,[1] Jinping Yao,[2,*] Zhaoxiang Liu,[2,3] Jinming Chen,[2,4] Bo Xu,[2,3] Kang Lin,[1] Junjie Qiang,[1] Boqu He,[1] Huailiang Xu,[1] Ya Cheng,[1] Heping Zeng,[1] and Jian Wu[1,†]

[1]*State Key Laboratory of Precision Spectroscopy, East China Normal University, Shanghai 200062, China*

[2]*State Key Laboratory of High Field Laser Physics, Shanghai Institute of Optics and Fine Mechanics, Chinese Academy of Sciences, Shanghai 201800, China*

[3]*University of Chinese Academy of Sciences, Beijing 100049, China*

[4]*School of Physical Science and Technology, ShanghaiTech University, Shanghai 200031, China*

(Received 21 December 2018; published 15 May 2019)

We experimentally investigate air lasing emission from singly ionized nitrogen molecules exposed to bicircular two-color (BTC) femtosecond laser pulses. The light driven electron recollision is suppressed in the corotating BTC field as compared to the counter-rotating one. It allows us to straightforwardly examine the role of electron recollision on the air lasing generation by simply changing the rotating sense of the BTC fields. Lasing emission is observed for both corotating and counter-rotating BTC fields without noticeable difference when the rotating sense is switched from one to the other case. It indicates a minor contribution of electron recollision on the air lasing emission. In addition to the well-observed linear polarization, we demonstrate that the polarization of the newborn lasing emission can be remotely manipulated from linear to circular by controlling the polarization of the driving second-harmonic field which at the same time acts as the seed.

DOI: 10.1103/PhysRevA.99.053413

Air lasing emission by launching intense ultrashort laser pulses in atmosphere opens exciting perspectives for interesting applications, e.g., standoff spectroscopy [1], detection of pollutants [2], and diagnosis of molecular dynamics [3–5]. Both backward and forward lasing emissions along the propagation direction of the driven light have been observed based on various mechanisms [6–15]. For instance, lasing emissions from nitrogen or oxygen atoms were launched via two-photon dissociation of the molecules and subsequent resonant two-photon excitation of the ejected atomic fragments by ultraviolet laser fields [6–8]. The collisional excitation by hot electrons plays an important role in the observed lasing emission from neutral nitrogen molecules (N_2) [13]. Unlike lasing actions from atoms and neutral molecules, the physical mechanism of N_2^+ lasing is under hot debate [16–26]. Two different scenarios were suggested to understand the population increase of the excited states of the photoionization-created N_2^+, i.e., the electron recollision induced excitation [17,18] and the dipole-allowed photon-coupled transitions among various states [19,20]. The electron recollision scenario was proposed by the observed similar dependence on the ellipticity of the driving light as the high-harmonic generation [17], and supported by its high sensitivity on the pulse duration and the central wavelength of the driving light [18]. Nevertheless, lasing emission was also observed in recent experiments driven by a circularly polarized pulse [24], which indicates that recollision does not play a significant role in the N_2^+ lasing emission. The conflicting conclusion makes us puzzling in regard to the electron recollision scenario.

In this paper, we propose a straightforward experiment to examine the role of the electron recollision in the air lasing emission from singly ionized N_2 driven by bicircular two-color (BTC) laser fields. The rotating sense of the BTC fields is switched between corotating and counter-rotating without changing the temporal durations and intensities of the two colors. The motion of the photoelectron is extremely sensitive to the polarization of the laser fields. In general, the photoelectron will be deflected away from the parent ionic core in circularly polarized laser fields. However, by superimposing another circularly polarized laser field of different wavelength and rotating sense, the photoelectron motion will be altered. Light-driving electron recollision is expected for the counter-rotating BTC field, which is suppressed for the corotating case [27–29]. Our experimental results indicate a minor contribution of the electron recollision to the newborn lasing emission because of its weak dependence on the rotating sense of the driving BTC fields. The photoionization of N_2 will mostly populate the ground state of N_2^+ which may further be coupled to the excited states via the dipole-allowed transitions for the subsequently emitted lasing. The intensity of the generated air lasing can be optimized by adjusting the relative strength between the two colors of the driving BTC fields. Interestingly, the polarization of the newborn lasing closely follows that of the seed in the input two-color fields, allowing us to remotely produce circularly or elliptically polarized lasing emission in addition to the well-observed linear polarization.

As schematically illustrated in Fig. 1(a), we create BTC laser fields with adjustable polarizations and intensities. The laser pulses propagate along the x axis, and polarize in the y-z plane. A linearly polarized femtosecond laser pulse (40 fs, 800 nm, 1 kHz) from a Ti:sapphire amplifier is frequency doubled

*jinpingmrg@163.com
†jwu@phy.ecnu.edu.cn

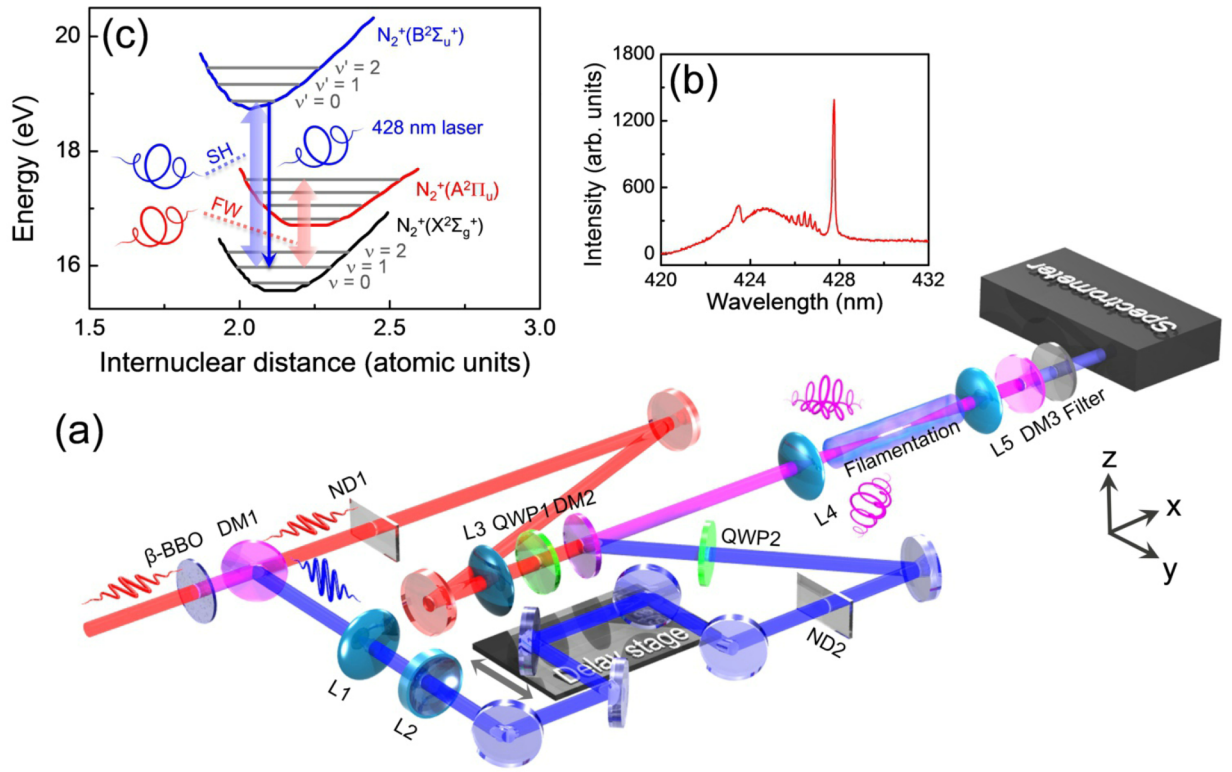

FIG. 1. (a) Schematic diagram of the experimental setup. (b) Spectrum of the forward lasing emission peaked at 428 nm. (c) Energy-level diagram of ionized nitrogen molecules in which the transition between $B^2\Sigma_u^+$ and $X^2\Sigma_g^+$ states corresponding to the 428-nm wavelength is indicated.

in a β-BBO crystal to produce a second-harmonic (SH) pulse at 400 nm. The SH beam and the fundamental-wave (FW) beam are split into two arms using a dichroic mirror (DM1). In each arm, a quarter-wave plate (QWP) is employed to individually adjust the polarization of the FW and SH fields. A motorized delay line stage is used to finely tune the temporal delay of the two beams. The relative intensity between FW and SH pulses is individually adjusted via two neutral density filters (i.e., ND1 and ND2) in the corresponding beam paths. The FW and SH fields are collinearly recombined to form a BTC laser field, which can be described as $\boldsymbol{E}(t) = \frac{1}{\sqrt{2}}[E_{\mathrm{FW}} f(t)\cos(\omega t) + E_{\mathrm{SH}} g(t)\cos(2\omega t)]\hat{\mathbf{e}}_y + \frac{1}{\sqrt{2}}[E_{\mathrm{FW}} f(t)\cos(\omega t + \phi_{\mathrm{FW}}) + E_{\mathrm{SH}} g(t)\cos(2\omega t + \phi_{\mathrm{SH}})]\hat{\mathbf{e}}_z$. The rotating sense of the BTC field is switched from corotating to counter-rotating by changing ϕ_{SH} from 0.5π to -0.5π for $\phi_{\mathrm{FW}} = 0.5\pi$. The BTC laser field is then focused by an $f = 10$ cm lens (L4) into a gas cell filled with 550-mbar N_2 molecules to generate a filament and coherent lasing emission. Here we focus on the air lasing emission centered at 428 nm. The residual FW and the accompanying supercontinuum background are blocked by a dichroic mirror (DM3) and a bandpass filter before the spectrometer (Shamrock 500i, Andor). As shown in Fig. 1(b), a strong lasing emission appears at 428 nm, which corresponds to the transition between $B^2\Sigma_u^+$ ($v' = 0$) and $X^2\Sigma_g^+$ ($v = 1$) states of N_2^+ [see the potential energy curves of the involved states in Fig. 1(c)]. The discrete peaks on the blue side of the lasing line originate from *R*-branch rotational transitions [3–5].

Figure 2(a) shows the measured intensity of the lasing emission at 428 nm versus the relative strength between the two colors, i.e., $E_{\mathrm{SH}}/E_{\mathrm{FW}}$, of the corotating (blue squares) and counter-rotating (red circles) BTC fields. The error bars in Fig. 2(a) are standard deviations of the signal intensities, which are calculated using the formula $D = \sqrt{\frac{\sum_{i=1}^{n}(x_i - \bar{x})^2}{n-1}}$, where n is the statistic number of the measurements; x_i and $\bar{x}$ are the individual value and the mean value of the data, respectively. Here, we keep the combined intensity $(1/2nc\varepsilon_0|E_{\mathrm{FW}} + E_{\mathrm{SH}}|^2)$ of the FW and SH fields of the BTC field constant ($\sim 4.6 \times 10^{14}$ W/cm^2) when their relative field strength ratio is varied. In the measurement, the zero time delay is chosen to examine the contribution of electron recollision. Regardless of the rotating sense of the BTC fields, our previous measurements [30] showed that the N_2^+ yield is almost the same for the constant combined intensity of the two colors. It allows us to exclude the influence of the single ionization process on the subsequent emitted lasing when the rotating sense and relative strength of the BTC field are altered. However, the photoelectron motion is extremely sensitive to the rotating sense of the BTC fields. In the counter-rotating BTC field, the electron has a decent probability to revisit its parent ion, which allows for the electron-ion recollision process to occur. In contrast, the corotating BTC field cannot efficiently drive the electron back to the parent ion, so the recollision process is suppressed. It is consistent with the fact that the electron recollision assisted dissociation or double ionization of the molecule showed noticeable enhancement for the counter-rotating BTC field as compared to the

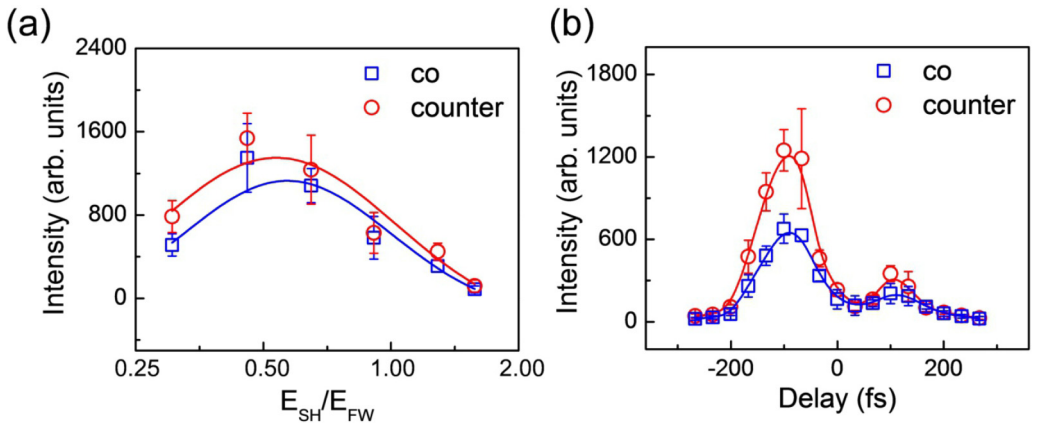

FIG. 2. (a) Experimentally measured intensity of the lasing signal at 428 nm versus the relative strength of the FW and SH fields for the corotating (blue squares) and counter-rotating (red circles) BTC fields. The solid curves are numerical fits to guide the eyes. (b) Experimentally measured intensity of the lasing signal at 428 nm as a function of the relative time delay between the corotating (or counter-rotating) circularly polarized FW and SH pulses. The strengths of the FW and SH fields are measured to be $I_{SH} = 2.6 \times 10^{13}$ W/cm^2 and $I_{FW} = 2.76 \times 10^{14}$ W/cm^2, respectively.

corotating one [30]. Here, as shown in Fig. 2(a), the intensity of the newborn 428-nm lasing emission is almost the same within the error bars of the measurements when we switched the rotating sense of the BTC fields from corotating (blue squares) to counter-rotating (red circles). It clearly excludes the important role of the light driving electron recollision, if there is any, on the observed air lasing emission from the singly ionized molecules.

As shown in Fig. 2(a), the intensity of the lasing emission depends on the relative strength between the FW and SH fields. The 428-nm lasing emission is maximal when $E_{SH}/E_{FW} \sim 0.5$, which drops when the relative strength of the SH and FW fields is detuned. Since the N_2^+ yield only weakly depends on the field ratio of E_{SH}/E_{FW} [30], the here observed E_{SH}/E_{FW}-dependent lasing emission might be caused by the dipole-allowed photon-coupled transitions among the ground and excited states of the photoionization created N_2^+. By removing one electron from the highest occupied molecular orbital of N_2, the photoionization created N_2^+ mostly populates on the $X\,^2\Sigma_g^+$ ground state, which can be further coupled to the excited states of $A\,^2\Pi_u$ or $B\,^2\Sigma_u^+$ by additionally absorbing one FW or SH photon from the two-color laser fields as schematically illustrated in Fig. 1(c). To create the coherent emissions between the $B\,^2\Sigma_u^+$ and $X\,^2\Sigma_g^+$ states, a depletion of the $X\,^2\Sigma_g^+$ state by coupling it to the $A\,^2\Pi_u$ state is also very important. By reducing the relative strength of the FW field, the transition from $X\,^2\Sigma_g^+$ to $A\,^2\Pi_u$ is decreased, which reduces the probability of lasing emissions between the $B\,^2\Sigma_u^+$ and $X\,^2\Sigma_g^+$ states. The SH field causes the transition of the population back and forth between the $B\,^2\Sigma_u^+$ and $X\,^2\Sigma_g^+$ states, depending on the relative population on these two states. When the SH field is too weak, for instance, $E_{SH}/E_{FW} \sim 0.3$, the population on the $B\,^2\Sigma_u^+$ state is not significant and thus the lasing emission is weak as shown in Fig. 2(a). Therefore there is an optimal ratio of E_{SH}/E_{FW} ($\sim$0.5 in our experiments) which maximizes coherent emissions between the $B\,^2\Sigma_u^+$ and $X\,^2\Sigma_g^+$ states. Since the single ionization of N_2 is driven by the same laser pulse, the photon-coupled transitions among various states of photoionization created N_2^+ would mostly occur at the tail of the BTC fields.

As previously demonstrated using linearly polarized pulses [5,31], the air lasing emission is enhanced at a nonzero time delay between the intense FW pump pulse and weak SH seed pulse. As shown in Fig. 2(b), here we observe similar enhancement of the 428-nm lasing emission by tuning the relative time delay between the circularly polarized FW and SH pulses. The positive delay corresponds to the SH pulse lags behind the FW pulse. Here the relative field ratio of E_{SH}/E_{FW} is set to be 0.3. In both counter-rotating and corotating cases, we can clearly observe two enhancements of the lasing emission around $\pm$100 fs. It could be the consequence of the interaction of the probe pulse with molecules prealigned by the pump pulse. Impulsively kicked by a circularly polarized femtosecond laser pulse, the molecules will be aligned in the polarization plane after the conclusion of the pump pulse [32]. When the probe pulse polarized in the same plane arrives at the alignment instant (around 100 fs after the pump pulse for the room temperature N_2), the ionization probability of the N_2 molecules will increase and lead to the enhancement of the subsequent lasing emission from the photoionization created N_2^+. Meanwhile, the dipole-allowed transitions from the $X\,^2\Sigma_g^+$ to $B\,^2\Sigma_u^+$ (or $A\,^2\Pi_u$) states are optimal for molecules when the molecular axis is parallel (or perpendicular) to the laser field. This also increases the lasing emission from N_2^+ around $\pm$100 fs where the molecules are aligned in the polarization plane of the time-delayed probe pulse of circular polarization. In our two-color field scheme, the intense FW pulse at 800 nm is the dominating pulse to excite the molecule and generate the lasing. At a time delay of -100 fs, the SH pulse aligns the molecules and the later arrived FW pulse produces the lasing emission seeded with the weak tail of the SH pulse, which is more efficient as compared to the $+100$ fs time delay where the relative weak SH pulse acts as the driving pulse for the newborn lasing from the impulsively aligned molecules.

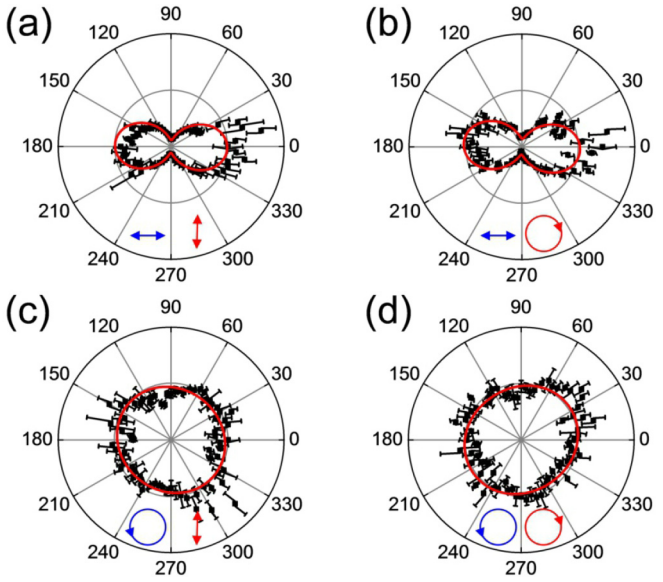

FIG. 3. (a–d) Experimentally measured polarization states of the 428-nm lasing signal driving by two-color fields of various polarizations. The strengths of the FW and SH fields here are measured to be $I_{SH} = 2.6 \times 10^{13}\,W/cm^2$ and $I_{FW} = 2.76 \times 10^{14}\,W/cm^2$, respectively, and the delay of the two pulses is at zero time delay.

The relatively higher lasing signal driven by the counter-rotating BTC field than that by the corotating one at nonzero time delays, as shown in Fig. 2(b), might relate to the field rotating sense–dependent selective excitation of the molecules, which has been previously observed in strong-field ionization of atoms [33]. The electron in the orbital with magnetic quantum number $m = -1$ (or $+1$) is preferred to be ionized by the right (or left) circularly polarized light. By employing two time-delayed circularly polarized pulses with opposite helicities, for instance, the pump preferably depletes the electron in the $+m$ sublevel and the probe will further ionize the $-m$ sublevel of the orbital. It is more efficient than the case when the pump and probe have the same helicity which preferably ionize the electron in the sublevel orbital of the same m. In analogy to atoms, the molecules exposed to time-delayed BTC pulses with opposite helicities are expected to have a higher probability to be excited for the subsequent lasing emission than that of the same helicity, as we observed in Fig. 2(b). Such effect should also exist at the zero time, but it is noticeably amplified when the molecules are prealigned in the polarization plane of the laser fields. A theoretical simulation is desired to visualize and get deep insights of this scenario.

Although linearly polarized air lasing is well observed driven by linearly polarized strong laser fields, the air lasing emission of circular polarization has not been reported, which is implicative for remote sensing of chiral dynamics of the molecules. Following the polarization state of the seed, here we demonstrate that the polarization of the newborn lasing emission can be tuned from linear to circular by manipulating the polarizations of the driving two-color fields as shown in Fig. 3. The polarizations of the input SH and FW pulses are denoted as blue and red directional circles or arrows at the bottom of the panels. The polarization of lasing emission is examined by a polarizer placed before the spectrometer. As shown in Figs. 3(a) and 3(b), no matter whether the FW is linear or circular, the lasing emission is linearly polarized as that of the input SH pulse which acts as the seed. It indicates the mechanism of seed amplification because both spontaneous emission and amplified spontaneous emission will show isotropic polarization. Interestingly, as shown in Figs. 3(c) and 3(d), circularly polarized lasing emission is generated when the input SH field is close to circular regardless of the polarization of the FW field. By fitting the measured data in Figs. 3(c) and 3(d), the ellipticity of the lasing emission can reach 0.95 and 0.94, respectively. Furthermore, the rotating sense of the newborn circularly polarized lasing emission closely follows that of the seed SH field. As we experimentally checked (data not shown here), after a quarter-wave plate the circular lasing emission was changed to linear along the same direction as that of the circularly polarized seed SH field after a quarter-wave plate. This denotes that the rotating sense of the lasing emission is in accordance with the seed SH field. By manipulating the rotating sense of the driving two-color fields, we can readily control the polarization of the newborn lasing emission for multifarious applications.

In summary, we adopt a BTC laser field with controllable rotating sense to examine the role of the electron recollision in the air lasing generation from singly ionized N_2 molecules. By switching the BTC laser fields from corotating to counter-rotating, no noticeable enhancement of the intensity of the newborn laser emission is observed, indicating the minor role of the electron recollision in the present experiments, if there is any. For a constant combined intensity of the driving BTC fields, the yield of air lasing emission is optimal by adjusting the relative strength of the two colors. It relates to the efficient couplings between the excited and ground states of the photoionization created N_2^+ induced by the dipole-allowed transitions among them. In additional to the well-observed linear polarization, circularly polarized air lasing emission is directly produced with controllable rotating sense by following that of the input SH field which acts as the seed. This work not only helps us to understand the mechanism of air lasing generation of singly ionized nitrogen molecules, but also provides a route for remote creation of the circularly polarized air lasing.

We acknowledge Feng He for fruitful discussions. This work was supported by the National Key R&D Program of China (Grant No. 2018YFA0306303); the National Natural Science Fund (Grants No. 11425416, No. 11761141004, No. 11822410, No. 11621404, and No. 61575211); Project of Shanghai Committee of Science and Technology (Grant No. 17JC1400400).

[1] P. R. Hemmer, R. B. Miles, P. Polynkin, T. Siebert, A. V. Sokolov, P. Sprangle, and M. O. Scully, Proc. Natl. Acad. Sci. USA **108**, 3130 (2011).

[2] P. N. Malevich, R. Maurer, D. Kartashov, S. Ališauskas, A. A. Lanin, A. M. Zheltikov, M. Marangoni, G. Cerullo, A. Baltuška, and A. Pugžlys, Opt. Lett. **40**, 2469 (2015).

[3] H. Zhang, C. Jing, J. Yao, G. Li, B. Zeng, W. Chu, J. Ni, H. Xie, H. Xu, S. L. Chin, K. Yamanouchi, Y. Cheng, and Z. Xu, Phys. Rev. X **3**, 041009 (2013).
[4] H. Xie, B. Zeng, G. Li, W. Chu, H. Zhang, C. Jing, J. Yao, J. Ni, Z. Wang, Z. Li, and Y. Cheng, Phys. Rev. A **90**, 042504 (2014).
[5] M. Lei, C. Wu, A. Zhang, Q. Gong, and H. Jiang, Opt. Express **25**, 4535 (2017).
[6] A. Dogariu, J. B. Michael, M. O. Scully, and R. B. Miles, Science **331**, 442 (2011).
[7] A. Laurain, M. Scheller, and P. Polynkin, Phys. Rev. Lett. **113**, 253901 (2014).
[8] A. Dogariu and R. B. Miles, in *Conference on Lasers and Electro-optics CLEO*, OSA Technical Digest (Optical Society of America, Washington, DC, 2013), paper QW1E.1.
[9] V. A. Vaulin, V. N. Slinko, and S. S. Sulakshin, Sov. J. Quantum Electron. **18**, 1457 (1988).
[10] Q. Luo, W. Liu, and S. L. Chin, Appl. Phys. B **76**, 337 (2003).
[11] D. Kartashov, S. Ališauskas, G. Andriukaitis, A. Pugžlys, M. Shneider, A. Zheltikov, S. L. Chin, and A. Baltuška, Phys. Rev. A **86**, 033831 (2012).
[12] D. Kartashov, S. Ališauskas, A. Baltuška, A. Schmitt-Sody, W. Roach, and P. Polynkin, Phys. Rev. A **88**, 041805(R) (2013).
[13] S. Mitryukovskiy, Y. Liu, P. Ding, A. Houard, and A. Mysyrowicz, Opt. Express **22**, 12750 (2014).
[14] J. Yao, B. Zeng, H. Xu, G. Li, W. Chu, J. Ni, H. Zhang, S. L. Chin, Y. Cheng, and Z. Xu, Phys. Rev. A **84**, 051802(R) (2011).
[15] J. Yao, G. Li, C. Jing, B. Zeng, W. Chu, J. Ni, H. Zhang, H. Xie, C. Zhang, H. Li, H. Xu, S. L. Chin, Y. Cheng, and Z. Xu, New J. Phys. **15**, 023046 (2013).
[16] J. Ni, W. Chu, C. Jing, H. Zhang, B. Zeng, J. Yao, G. Li, H. Xie, C. Zhang, H. Xu, S. L. Chin, Y. Cheng, and Z. Xu, Opt. Express **21**, 8746 (2013).
[17] Y. Liu, P. Ding, G. Lambert, A. Houard, V. Tikhonchuk, and A. Mysyrowicz, Phys. Rev. Lett. **115**, 133203 (2015).
[18] Y. Liu, P. Ding, N. Ibrakovic, S. Bengtsson, S. Chen, R. Danylo, E. R. Simpson, E. W. Larsen, X. Zhang, Z. Fan, A. Houard, J. Mauritsson, A. L'Huillier, C. L. Arnold, S. Zhuang, V. Tikhonchuk, and A. Mysyrowicz, Phys. Rev. Lett. **119**, 203205 (2017).
[19] J. Yao, S. Jiang, W. Chu, B. Zeng, C. Wu, R. Lu, Z. Li, H. Xie, G. Li, C. Yu, Z. Wang, H. Jiang, Q. Gong, and Y. Cheng, Phys. Rev. Lett. **116**, 143007 (2016).
[20] H. Xu, E. Lötstedt, A. Iwasaki, and K. Yamanouchi, Nat. Commun. **6**, 8347 (2015).
[21] S. L. Chin, H. Xu, Y. Cheng, and Z. Xu, Chin. Opt. Lett. **11**, 013201 (2013).
[22] A. Azarm, P. Corkum, and P. Polynkin, Phys. Rev. A **96**, 051401(R) (2017).
[23] D. Kartashov *et al.*, in *Research in Optical Sciences*, OSA Technical Digest (Optical Society of America, Washington, DC, 2014), paper HTh4B.5.
[24] M. Britton, P. Laferrière, D. H. Ko, Z. Li, F. Kong, G. Brown, A. Naumov, C. Zhang, L. Arissian, and P. B. Corkum, Phys. Rev. Lett. **120**, 133208 (2018).
[25] Z. Liu, J. Yao, J. Chen, B. Xu, W. Chu, and Y. Cheng, Phys. Rev. Lett. **120**, 083205 (2018).
[26] L. Arissian, B. Kamer, A. Rastegari, D. M. Villeneuve, and J. C. Diels, Phys. Rev. A **98**, 053438 (2018).
[27] K. J. Yuan and A. D. Bandrauk, Phys. Rev. A **92**, 063401 (2015).
[28] C. A. Mancuso, K. M. Dorney, D. D. Hickstein, J. L. Chaloupka, J. L. Ellis, F. J. Dollar, R. Knut, P. Grychtol, D. Zusin, C. Gentry, M. Gopalakrishnan, H. C. Kapteyn, and M. M. Murnane, Phys. Rev. Lett. **117**, 133201 (2016).
[29] S. Eckart, M. Richter, M. Kunitski, A. Hartung, J. Rist, K. Henrichs, N. Schlott, H. Kang, T. Bauer, H. Sann, L. Ph. H. Schmidt, M. Schöffler, T. Jahnke, and R. Dörner, Phys. Rev. Lett. **117**, 133202 (2016).
[30] K. Lin, X. Jia, Z. Yu, F. He, J. Ma, H. Li, X. Gong, Q. Song, Q. Ji, W. Zhang, H. X. Li, P. Lu, H. Zeng, J. Chen, and J. Wu, Phys. Rev. Lett. **119**, 203202 (2017).
[31] X. Zhong, Z. Miao, L. Zhang, Q. Liang, M. Lei, H. Jiang, Y. Liu, Q. Gong, and C. Wu, Phys. Rev. A **96**, 043422 (2017).
[32] C. Smeenk and P. B. Corkum, J. Phys. B: At., Mol. Opt. Phys. **46**, 201001 (2013).
[33] T. Herath, L. Yan, S. K. Lee, and W. Li, Phys. Rev. Lett. **109**, 043004 (2012).